

Evaluation of heat resistance of SiC-based ceramic fibers via *in situ* elastic modulus and electrical conductivity measurement at elevated temperatures

Kazuya Shimoda^{a,b*}, Christian Colin^a

^a DEN/DANS/DMN/SRMA, Commissariat à l'Énergie Atomique de Saclay (CEA-Saclay), Gif-sur-Yvette Cedex 91191, France.

^b Research Center for Structural Materials, National Institute for Materials Science (NIMS), 1-2-1 Sengen, Tsukuba, Ibaraki 305-0047, Japan.

*Corresponding author. At present: Research Center for Structural Materials, National Institute for Materials Science, 1-2-1 Sengen, Tsukuba, Ibaraki 305-0047, Japan. Tel.: +81 29 859 2306; Fax: +81 29 859 2401

E-mail address: SHIMODA.Kazuya@nims.go.jp (K. Shimoda)

**Abbreviations. PCS: polycarbosilane; SiC_f/SiC: SiC fiber-reinforced SiC matrix; FCIs: flow channel insets; N: Nicalon; HN: Hi-Nicalon; HNS: Hi-Nicalon Type S; TySA3: Tyranno-SA grade-3; FE-SEM: field emission scanning electron microscopy; EDS: energy dispersive X-ray spectroscopy; XRD: X-ray diffraction;

Abstract

SiC-based ceramic fibers have numerous applications as reinforcement materials. Herein, the *in situ* thermal stability of four types of SiC-based ceramic fibers from three generations was investigated in terms of elastic modulus and electrical conductivity at temperatures up to 1800 °C in a vacuum under low pressure ($<10^{-4}$ Pa). A specific tensile test device (MacaSiC) for single fibers was used. Mechanical and physical properties were monitored during heating and cooling at 1200, 1500, and 1800 °C for 10 min. Fibers exposed at 1200, 1500, and 1800 °C for 10 min were evaluated by measuring tensile strength retention, and correlating them with fiber crystallinity and microstructural evolution. Third-generation fibers exhibited excellent thermal stability at temperatures up to 1800 °C. The strength degradation of the third-generation SiC fibers was associated with the enlargement of apparent β -SiC crystallites and carbonization caused by the release of Si in the annular region of the fibers.

Keywords: *Silicon carbide; Ceramic fiber; Mechanical property; Physical property; Microstructural analysis*

1. Introduction

The organic-to-inorganic conversion process is typically used to manufacture continuous ceramic fibers by heating organic fibers. Numerous ceramic fibers have been created through the organic-to-inorganic conversion process, such as carbon fibers from polyacrylonitrile and Si-C-N fibers from carbosilazanes. The SiC-based ceramic fibers are industrially manufactured through the conversion of polycarbosilane (PCS) via the process developed by Yajima et al. during the 1970s and 1980s [1]. SiC-based ceramic fibers have

developed rapidly from the first generation—which had excess of carbon and a high oxygen content and was amorphous—to the third generation, which is nearly stoichiometric and polycrystalline [2]. Nippon Carbon Co. Ltd. (Japan) has industrially manufactured first-generation (Si-C-O) fibers from PCS as continuous fibers. Subsequently, UBE Industries Ltd. (Japan) has industrially manufactured first-generation (Si-Ti-C-O) fibers from polytitanocarbosilane. Conventional (first-generation) SiC-based ceramic fibers, sold under the names of Si-C-O fibers (NL-202 of Nicalon) and Si-Ti-C-O fibers (Lox-M of Tyranno), are heat-resistant up to 1200 °C and have been used as a reinforcement material for glass-ceramic matrix composites and aluminum wire materials [3–6]. Over the last few years, research has been conducted to enhance the high-temperature resistance of polymers converted to SiC ceramics and the thermal stability of the fibers at temperatures above 1300 °C. These studies revealed that a decrease in the oxygen content of the fiber was essential. Okamura et al. developed a new fabrication process known as radiation curing [7]. These studies have successfully produced new SiC-based ceramic fibers with a low oxygen content. The second-generation fibers are Hi-Nicalon, Tyranno Low-E, and Low-ZE, which have a high thermal resistance of approximately 1500 °C [3, 8]. Recently, SiC-based ceramic fibers with extraordinary thermal resistance at temperatures above 1700 °C have been produced on an industrial scale, and these fibers have a nearly stoichiometric composition of SiC with a highly crystalline structure. The third-generation fibers, such as Sylramic, Hi-Nicalon Type S, and Tyranno-SA, are employed as reinforcements for SiC matrix composites, i.e., SiC-fiber-reinforced SiC matrix (SiC_f/SiC) materials [9–15]. SiC_f/SiC composite materials have the potential to be used as high-performance structural materials/components in next-generation nuclear fission and fusion reactors [16]. For

example, these materials could be used for accident-tolerant fuel assemblies, applied to the fuel cladding and channel box of light water reactors, or for the blanket first wall or flow channel insets (FCIs) of fusion reactors [17–20]. FCIs are important components serving as electrical and thermal insulators, which are proposed to mitigate the magnetohydrodynamic pressure drop and increase coolant outlet temperature, employing liquid LiPb as both the breeding material and coolant in a dual coolant blanket concept for fusion reactors [17, 18]. Additionally, SiC_f/SiC composite materials are being developed for use in gas turbines for aerospace/aircraft and power generation applications, such as combustors, transition ducts, nozzles, flame holders, and exhaust liners [21–24]. To enable the successful development of SiC_f/SiC composite materials for these applications, the effects of high temperature on their mechanical and physical properties must be elucidated. It is well-known that the thermo-mechanical/physical performance of the composites is heavily reliant on the characteristics of the reinforcing fibers employed. Therefore, SiC-based ceramic fibers used as reinforcements should be thermally stable and maintain their approximate mechanical/physical properties even at elevated temperatures. Also, electrical conductivity must be kept as low as possible (less than 100 S/m) for FCI applications [17, 18]. However, information on the thermo-mechanical/physical and electrical properties of SiC-based ceramic fibers as a reinforcement at elevated temperatures has been scarce thus far owing to the difficulty in the measurement of these properties. Consequently, the ability to retain the original values (at room temperature, 25 °C) of tensile strength/elastic modulus, electrical conductivity, and microstructural changes after high-temperature exposure determines the heat resistance of the SiC-based ceramic fibers, as previously discussed. This study explored a novel technique to investigate the heat resistance of SiC-based ceramic fibers by

utilizing *in situ* measurement of the elastic modulus and electrical conductivity of a single fiber at elevated temperatures. Additionally, this research helps to improve our comprehension of the thermo-mechanical/physical stability of fuel-cladding tubes and the thermo-electrical performance of FCIs in service. Furthermore, the microstructural characteristics and tensile strength of the fibers after heat treatment were studied and compared to previously reported results under similar test temperature conditions.

2. Experimental procedure

2.1. Materials

This study evaluated four types of commercially available SiC-based ceramic fibers from three generations. The fibers used were Nicalon (N) with low electrical resistivity, Hi-Nicalon (HN), Hi-Nicalon Type S (HNS) from NGS Advanced Fibers Co. Ltd. (Toyama, Japan), and Tyranno-SA grade-3 (TySA3) from Ube Industry Ltd. (Ube, Japan). The characteristics of the fibers as provided by the manufacturer are outlined in Table 1. Typical properties of various SiC-based ceramic fibers are described in the recent reviews provided by Bunsell et al. and Wang et al. [2, 10]. The diameter and elemental composition of the fibers, which were provided by manufacturers, were almost identical to those in the reviews, but the tensile properties were slightly higher.

Table 1. Characteristics of various SiC-based ceramic fibers (data provided by manufacturers).

| | Nicalon | Hi-Nicalon | Hi-Nicalon | Tyranno-SA 3 rd |
|--|---------|------------|------------|----------------------------|
|--|---------|------------|------------|----------------------------|

| | with low electrical resistivity (N) | (HN) | Type S (HNS) | (TySA3) |
|-----------------------------|--|------------------------------------|---------------------|--|
| Diameter (μm) | 14 | 14 | 12 | 7.5 |
| Density (g/cm^3) | 2.4 | 2.65 | 2.85 | 3.1 |
| Atomic composition | $\text{SiC}_{1.34}\text{O}_{0.36}$ | $\text{SiC}_{1.39}\text{O}_{0.01}$ | $\text{SiC}_{1.05}$ | $\text{SiC}_{1.08}, \text{O}, \text{Al}_{<0.01}$ |
| Crystal state | Amorphous | Micro crystal | Crystalline | Crystalline |
| Tensile strength (GPa) | 3.1 | 3.2 | 3.1 | 2.51 |
| Tensile modulus (GPa) | 190 | 270 | 380 | 409 |

2.2 Experimental device set-up and in situ measurement at elevated temperatures

A specific device, named MacaSiC, was used to perform the *in situ* tensile tests of single fibers from room temperature (25 °C) to elevated temperatures (approximately 2000 °C). Fig. 1 illustrates a schematic of MacaSiC. The fibers were heated by an electrical current circulating through the fibers in a vacuum under a total pressure of less than 10^{-4} Pa. A pyrometer was used to measure the temperature of the fibers at temperatures above 1200 °C. Owing to the small diameter of the fibers (approximately 7.5 μm for TySA3 fibers; approximately 14 μm for N, HN, and HNS fibers), the pyrometer could only be used to measure the temperature of the fibers at temperatures above 1200 °C. When the temperature is below 1200 °C, the fiber temperature (T^*) (in K) can be estimated by the

following equation.

$$P_{\text{elec}} = \sigma \epsilon F S \times (T^*{}^4 - T_R^4), \quad (1)$$

where P_{elec} is the supplied electrical power; σ is the Stefan constant; ϵ is the fiber emissivity (equal to 1 in our case); F is the shape factor (equal to 1 in our case); S is the surface area of the specimens; and T_R is the room temperature in K (25 °C). The temperature profiles show that the temperature was uniform over more than 95% of the gauge length. Above 1200 °C, the discrepancy between the estimated and measured temperatures was under the conditions of <50 °C, and this is comparable to the measurement uncertainty attributed to the pyrometer. Before the tests, sizing agents were removed from all fibers under 600 °C for 30 min in a vacuum. *In situ* measurements of the elastic modulus and electrical conductivity of the various fibers during heating to elevated temperatures of up to 1800 °C were conducted via tensile tests of a single fiber with a gauge length of 25 mm. The fibers were attached to graphite grips using commercially available UCAR-grade C-34 carbonaceous cement. The section area of the fibers was circular, so that the mean diameter of the fibers (five measurements along the fibers) was measured before the tests using a laser diffraction technique [25]. At each temperature, two successful tensile tests were conducted for each fiber up to approximately 300 MPa at a strain rate of 10^{-4} 1/s. The mean elastic modulus was evaluated from the stress–strain curves in the elastic range between 20 and 300 MPa. The electrical conductivities of the fibers (θ) at different temperatures can be calculated from the current and voltage values of the electrical power supply used to heat the fiber using the following equation.

$$\theta = \frac{1}{\rho} = \frac{I}{V} \times \frac{L_0}{S_0}, \quad (2)$$

where ρ is the resistivity of the fiber; I is the electrical current; V is the electrical voltage; L_0 is the length of the fiber; and S_0 is the cross-sectional area of the fiber. *In situ* measurements of the elastic modulus and electrical conductivity of the fibers during heating and cooling treatments at maximum temperatures of 1200, 1500, and 1800 °C for a holding time of 10 min were performed in a vacuum under a total pressure of less than 10^{-4} Pa. The tensile strengths of the various fibers after heating and cooling at 1200, 1500, and 1800 °C were evaluated by tensile testing at a strain rate of 10^{-4} 1/s. Furthermore, the four types of fibers were thermally exposed in an electric furnace on a high-purity alumina boat to maximum temperatures of 1200, 1500, and 1800 °C for a holding time of 10 min in a vacuum under a total pressure of less than 10^{-4} Pa. The weight changes of the different fibers before and after exposure were measured on an electric balance (AP224X, Shimadzu, Japan) with an accuracy of 0.0001 g. The microstructural evolution of the fibers on the cross-section and surface before and after exposure was observed through field emission scanning microscopy (FE-SEM; S-4700, Hitachi, Japan) with energy dispersive X-ray spectroscopy (EDS). The crystalline phase was analyzed by X-ray diffraction (XRD; MiniFlex, Rigaku, Japan) using Cu-K α radiation. The scans were conducted for 2θ values of 10°–90°. The apparent size of the β -SiC crystallites was calculated from the half-value width of the (111) peak using Scherrer's formula. This apparent size of the β -SiC crystallites is likely considerably smaller than the actual grain size of the fibers because of the heavy twinning of the SiC crystals.

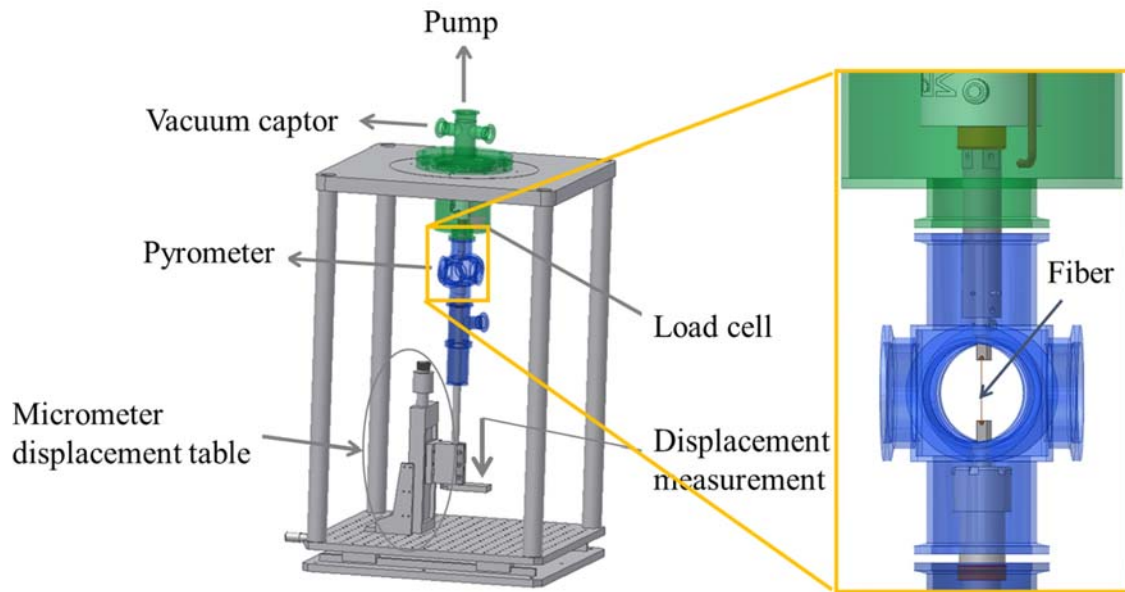


Fig. 1 Schematic of the specific tensile test device for a single fiber, referred to as MacaSiC.

3. Results

3.1. *In situ* measurement during heating up to 1800 °C

The mean diameter was 15.0 μm for N, 14.9 μm for HN, 12.7 μm for HNS, and 7.63 μm for TySA3. Fig. 2 shows the (a) elastic modulus and (b) normalized elastic modulus values of the SiC-based ceramic fibers when heated up to 1800 °C. At room temperature (25 °C), the elastic modulus was measured to be 179 ± 3.89 GPa for N, 271 ± 4.48 GPa for HN, 356 ± 1.84 GPa for HNS, and 396 ± 4.33 for TySA3. The mean values were obtained from the measurements obtained for at least 10 fibers. Fig. 3 shows the (a) electrical conductivity and (b) normalized electrical conductivity values of the various SiC-based fibers when heated up to 1800 °C. At room temperature (25 °C), the electrical

conductivity was measured to be 0.87 ± 7.27 S/m for N, 52.7 ± 0.01 S/m for HN, 80.3 ± 0.13 S/m for HNS, and 315 ± 0.18 S/m for TySA3. The mean values were obtained from the measurements obtained for at least 10 fibers. The elastic modulus and electrical conductivity values before testing (at room temperature, 25 °C) were the highest for TySA3 and the lowest for N. The elastic modulus values of the SiC-based ceramic fibers remained linear up to 1200 °C for N, 1300 °C for HN, 1300–1400 °C for HNS, and 1400 °C for TySA3. The electrical conductivity of the SiC-based ceramic fibers at elevated temperatures is strongly related to the elastic modulus. The elastic modulus of the N fiber exhibited a steep decline, whereas its electrical conductivity increased from 1200 °C. Thus, the electrical resistivity of the fiber was extremely low to induce resistive heating over 1400 °C; hence, conducting *in situ* measurements was difficult owing to the sudden rupture of the fiber. HN also exhibited a rapid decrease in the elastic modulus and an increase in electrical conductivity at approximately 1200 °C; however, the data were scattered owing to the instability of the fiber, thus avoiding the sudden rupture of the fiber over 1400 °C. The normalized electrical conductivity values of HN were smaller than those of N. The elastic modulus of HNS began to decrease gradually at 1400 °C, and the fiber retained approximately 40% of its original values (those at room temperature, 25 °C) even at 1800 °C. The behavior of the elastic modulus of HNS was comparable to that of TySA3 when heated near 1800 °C. The electrical conductivity values of HNS and TySA3 were lower than those of N and HN up to 1800 °C. However, the normalized electrical conductivity values of HNS were significantly higher than those of TySA3 at up to 1800 °C.

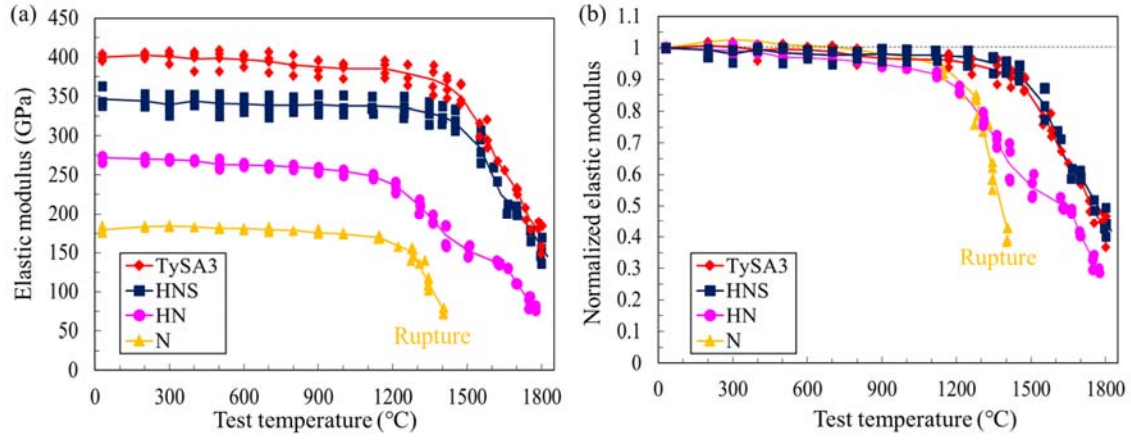


Fig. 2 (a) Elastic modulus and (b) normalized elastic modulus values of the various SiC-based ceramic fibers when heated up to 1800 °C.

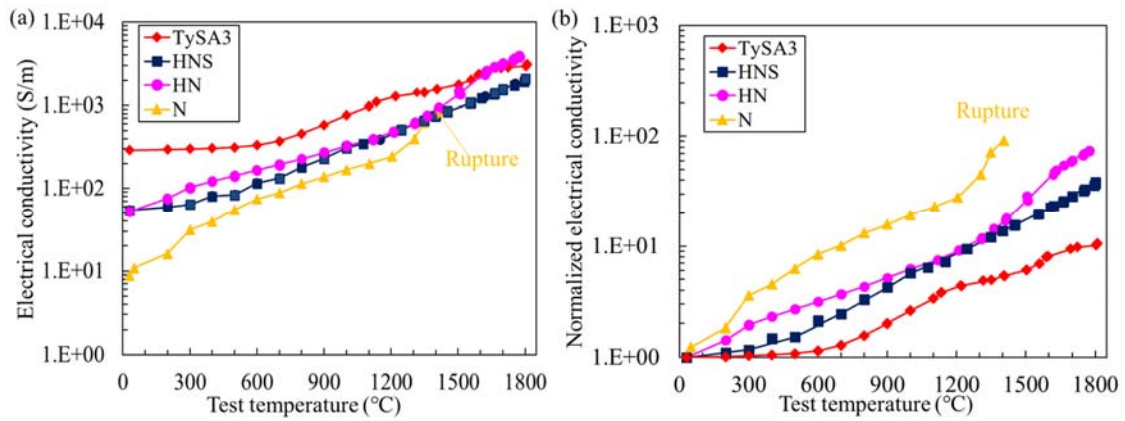


Fig. 3 (a) Electrical conductivity and (b) normalized electrical conductivity values of the various SiC-based ceramic fibers when heated up to 1800 °C.

3.2. In situ measurement during heating and cooling at 1200, 1500, and 1800 °C

Fig. 4 shows the variation in the elastic moduli and normalized elastic moduli of the SiC-based ceramic fibers during the heating and cooling treatments at the maximum temperatures of 1200, 1500, and 1800 °C for a holding time of 10 min. Solid and open symbols indicate the heating and cooling treatments, respectively. At 1200 °C, the elastic moduli of all the fibers during cooling were almost identical to those during heating without a sudden decline, which reacted reversibly. At temperatures higher than 1200 °C, the normalized elastic modulus values of N decreased rapidly, and the fiber underwent sudden rupture at around 1400 °C during heating. At 1500 °C, the elastic moduli of HN during cooling were higher than those during heating, and significantly increased during the holding time of 10 min at 1500 °C. Although the elastic modulus values of HNS and TySA3 began to gradually decrease at 1400 °C during heating, they were still comparable to the values observed during cooling. The normalized elastic modulus values of HNS and TySA3 remained at approximately 40% of the original values (those at room temperature, 25 °C) even at 1800 °C, and exhibited a marginal decrease after the heating and cooling treatments at 1800 °C. The elastic modulus of HNS and TySA3 after heating and cooling at 1800 °C for a holding time of 10 min was approximately 96% of the original values (those at room temperature, 25 °C).

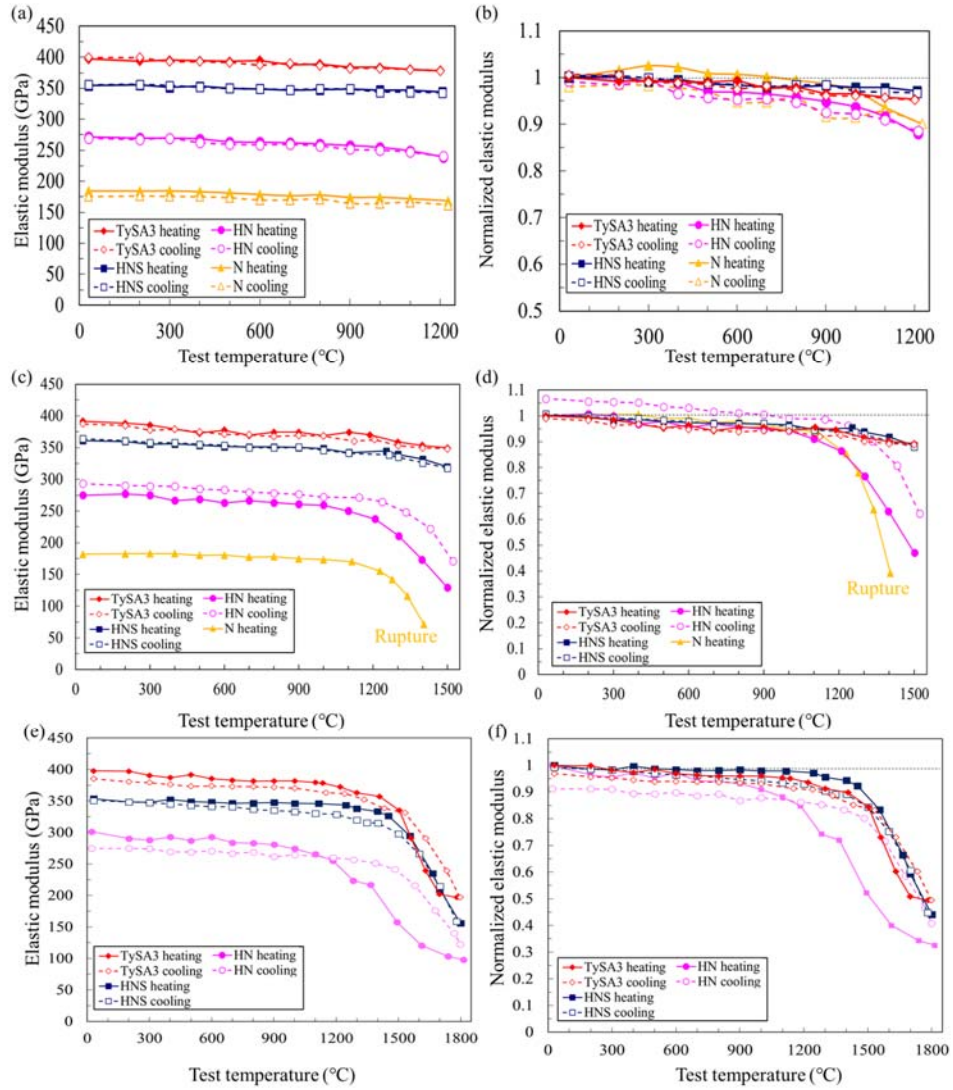


Fig. 4 Elastic moduli of the SiC-based ceramic fibers during heating and cooling treatments at the maximum temperature of (a) 1200, (c) 1500, and (e) 1800 °C for a holding time of 10 min; (b), (d), and (f) show the corresponding normalized elastic modulus values.

Fig. 5 shows the electrical conductivity and normalized electrical conductivity values of the SiC-based ceramic fibers during the heating and cooling treatments at the maximum temperatures of 1200, 1500, and 1800 °C for a holding time of 10 min. The

electrical conductivities of all the fibers increased gradually during heating up to 1200 °C, and the values during cooling were almost identical to those during heating. At 1200 °C, the normalized electrical conductivity of N during cooling was marginally higher than that during heating. The normalized electrical conductivity values of N increased sharply above 1200 °C, and the fiber underwent sudden rupture at around 1400 °C during heating. At 1500 °C, the normalized electrical conductivity of HN during cooling was higher than that during heating and the normalized electrical conductivity increased significantly during the holding time of 10 min at 1500 °C. The electrical conductivities of HNS and TySA3 began to increase gradually during heating and increased marginally during cooling. At 1800 °C, the electrical conductivity of HN increased significantly during the holding time of 10 min, and then increased marginally during cooling. The electrical conductivities of TySA3 and HNS increased gradually during heating up to 1800 °C. The normalized electrical conductivity values of HNS were greater than those of TySA3 during heating above 1200 °C. Nevertheless, during cooling below approximately 900 °C, the normalized electrical conductivity values of HNS were lower than those of TySA3.

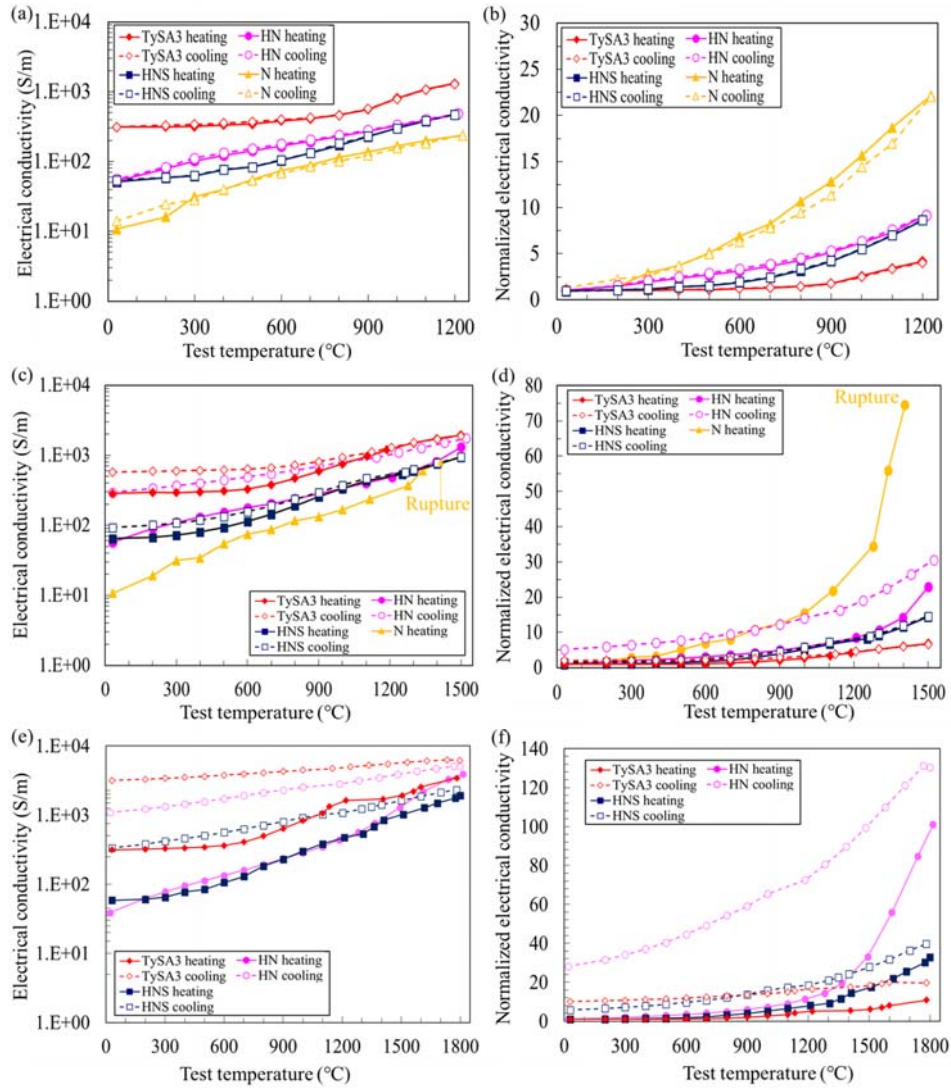


Fig. 5 Electrical conductivity of the SiC-based ceramic fibers during the heating and cooling treatments at the maximum temperature of (a) 1200, (c) 1500, and (e) 1800 °C for a holding time of 10 min; (b), (d), and (f) show the corresponding normalized electrical conductivity values.

3.3. Weight and strength changes after heating and cooling at 1200, 1500, and 1800 °C

After exposure to 1200 °C, weight losses of N and HN were 3.63% and 1.21%, respectively, whereas the others showed almost no change. After exposure to 1500 °C, weight losses of N, HN, HNS, and TySA3 were 25.6%, 2.93%, 0.815%, and 0.778%, respectively. After exposure to 1800 °C, weight losses of 21.9%, 19.1%, and 19.8% were observed for HN, HNS, and TySA3, respectively. Fig. 6 represents the (a) tensile strengths and (b) normalized tensile strengths of the SiC-based ceramic fibers after heating and cooling at 1200, 1500, and 1800 °C for 10 min. The tensile strength, determined using the single filament tensile test technique at room temperature (25 °C) using five fibers, was measured to be 2.81 ± 0.65 , 2.85 ± 0.55 , 2.68 ± 0.35 , and 2.24 ± 0.56 GPa for N, HN, HNS, and TySA3, respectively. The tensile strengths were slightly lower than the strengths provided by manufacturers as listed in Table 1. This may be due to the removal process of sizing agents; however, the measured values were mostly consistent with the data reported by Bunsell et al. and Wang et al. [2, 10]. Fig. 6 also shows the previously reported strength retention of HN, HNS, and TySA3 after exposure to various extremely low oxygen partial pressure conditions in Ar, Ar–O₂, and vacuum for 1 or 10 h [8, 26–28]. The tensile strength of N decreased at 1200 °C and subsequently declined until almost completely failing at 1500 °C. The tensile strength of HN decreased marginally at 1200 °C, and thereafter significantly decreased to approximately 40% of the original value (that at room temperature, 25 °C). HNS and TySA3 showed excellent strength retention up to 1500 °C. At 1800 °C, the tensile strength of HNS was marginally higher than that of TySA3.

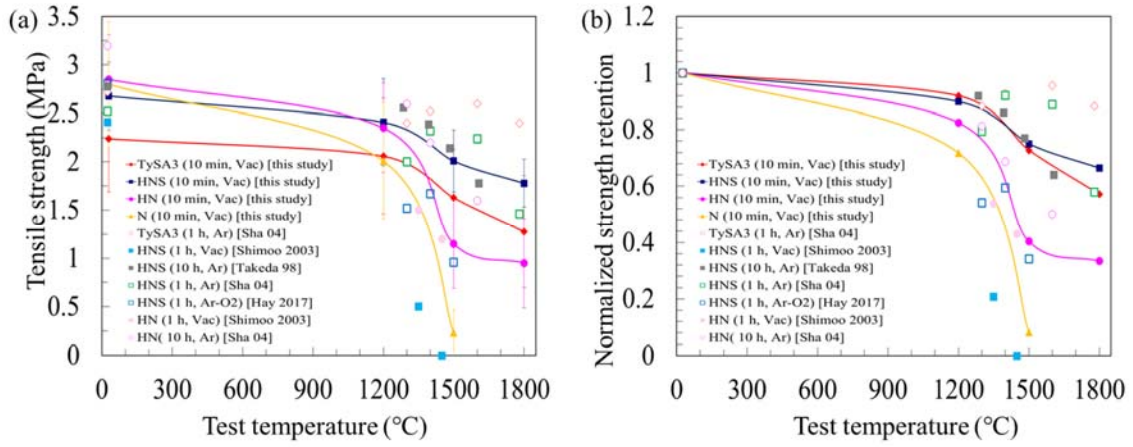


Fig. 6 (a) Tensile strength and (b) normalized tensile strength values of the SiC-based ceramic fibers after heating and cooling at 1200, 1500, and 1800 °C for 10 min.

3.4. Characterization of the fibers after exposure at 1200, 1500, and 1800 °C

3.3.1 Crystalline phase

Fig. 7 shows the XRD patterns of the SiC-based ceramic fibers before and after exposure at 1200, 1500, and 1800 °C for a holding time of 10 min in a vacuum. The XRD patterns of the fibers before exposure (at room temperature, 25 °C) show three main peaks, which were assigned to the (111), (220), and (311) planes of cubic SiC (β -SiC). The XRD patterns of N before exposure are very broad and exhibit a relatively high oxygen content, thus indicating that N has a low degree of crystallinity and is mainly composed of an amorphous phase. Thus, N has a mixture of nano-crystalline β -SiC with a calculated apparent crystallite size of 2.1 nm, free carbon, and an amorphous (Si-C-O) phase. The phases present in HN were nano-crystalline β -SiC with a calculated apparent crystallite size of 4.4 nm and free carbon. In comparison, the XRD patterns of HNS and TySA3 indicated the presence of highly crystalline β -SiC, and the calculated apparent crystallite sizes were

12.1 nm and 34.3 nm, respectively. The XRD patterns of HNS and TySA3 showed β -SiC peaks with planar defects (stacking faults and microtwins) at $2\theta = 35^\circ$ owing to their very high fabrication temperature (approximately 1600 °C for HNS and 1800 °C for TySA3). After exposure at temperatures greater than 1500 °C, three peaks were observed and the peak height increased with an increase in the exposure temperature. The observed peaks are indexed as the (111), (200), and (222) crystal planes and are visible in the patterns of HN. The diffraction peaks in N and HN became more distinct and narrower when the temperature was higher than 1200 °C, whereas they were not so clear for HNS and TySA3. A carbon peak at $2\theta = 26^\circ$ was detected in the XRD pattern of HN after exposure to temperatures greater than 1200 °C. The highly intense diffraction peaks of β -SiC in HNS and TySA3 before exposure (at room temperature, 25 °C) suggested that these fibers already had a highly crystallite structure owing to their very high fabrication temperature (approximately 1600 °C for HNS and 1800 °C for TySA3). When exposed to temperatures greater than 1500 °C, gradual crystallization of β -SiC occurred in HNS and TySA3. A plot of the apparent β -SiC (111) crystallite size as a function of the exposure temperature is shown in Fig. 8. Evidently from the plot, the grain growth in N and HN began at 1200 °C. Moreover, the apparent crystallite size of β -SiC in HNS and TySA3 stayed nearly the same at temperatures below 1500 °C, whereas exposure to higher temperatures caused a continuous increase in the apparent crystallite size of β -SiC in HNS. It appears that the apparent crystallite size of β -SiC in TySA3 fibers is not significantly affected by exposed temperatures. The apparent crystallite sizes of β -SiC in HN, HNS, and TySA3 after exposure at 1800 °C for a holding time of 10 min were 20.6, 23.9, and 38.7 nm,

respectively. In addition, the XRD pattern of TySA3 after exposure at 1800 °C revealed a carbon peak at $2\theta = 26^\circ$.

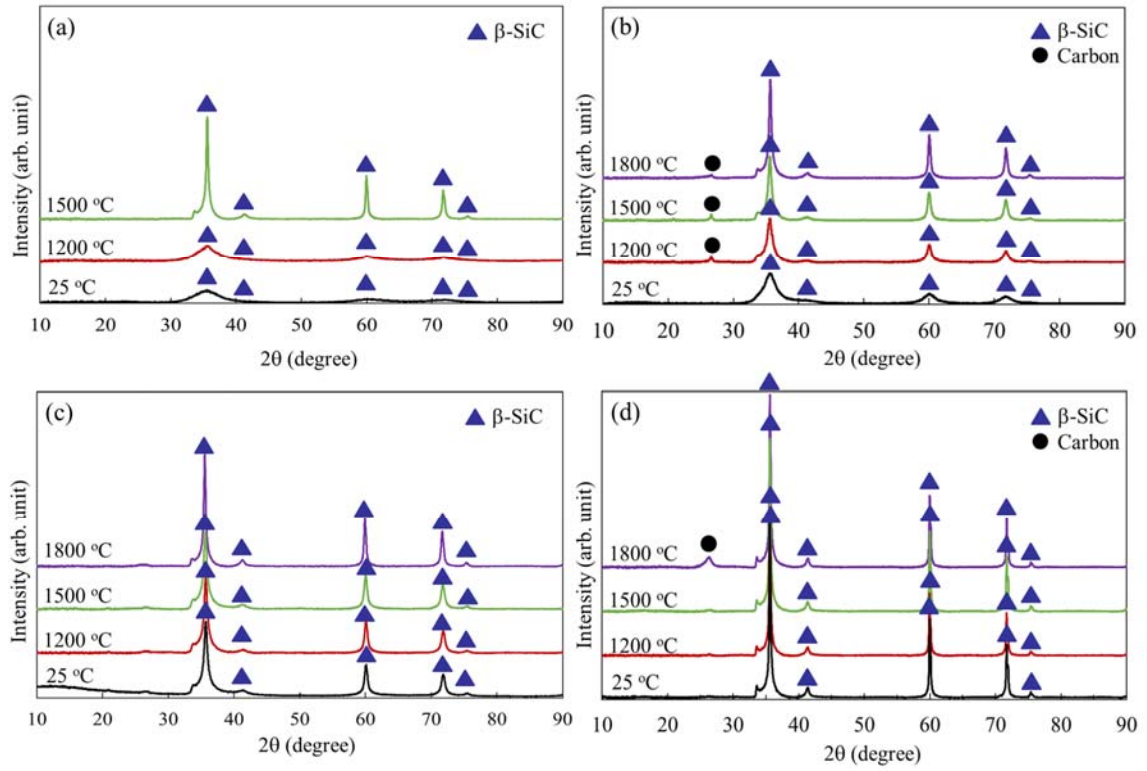


Fig. 7 XRD patterns of the SiC-based ceramic fibers before (25 °C) and after exposure to temperatures of 1200, 1500, and 1800 °C for a holding time of 10 min in a vacuum: (a) N, (b) HN, (c) HNS, and (d) TySA3.

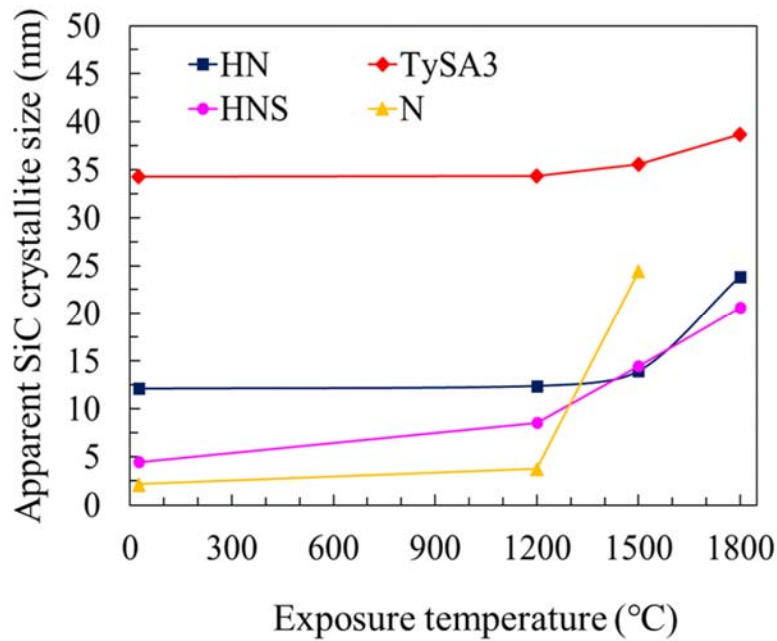


Fig. 8 Plot of the apparent β -SiC (111) crystallite size as a function of the exposure temperature.

3.3.2 Microstructural evolution

Fig. 9 shows the microstructural evolution of N before and after exposure to temperatures of 1200 and 1500 °C for a holding time of 10 min in a vacuum. The N fiber exposed at 1200 °C had a slightly porous structure in an annular region (Figs. 9(c)). Noticeable changes in appearance were observed in the fibers exposed at 1500 °C. The fibers showed a completely porous microstructure and its surface underwent coarsening (Fig. 9(e) and (f)). Fig. 10 shows the microstructural evolution of HN before and after exposure to temperatures of 1200, 1500, and 1800 °C for a holding time of 10 min in a vacuum. The HN fiber exposed at 1200 °C had a smooth surface and was largely identical to the fiber before exposure (Fig. 10(d)). Exposure to temperatures over 1500 °C caused a

coarsening of the fiber surface (Fig. 10(f)). Fig. 11 shows the microstructural evolution of HNS before and after exposure to temperatures of 1200, 1500, and 1800 °C for a holding time of 10 min in a vacuum. The microstructure of the HNS fibers exposed to temperatures below 1500 °C was comparable to that of the fibers before exposure (Fig. 11(d)). After exposure at 1800 °C, the fiber surface caused slight coarsening, and no structural degradation was observed at the core (Figs. 11(e) and (f)). Fig. 12 shows the microstructural evolution of TySA3 before and after exposure to temperatures of 1200, 1500, and 1800 °C for a holding time of 10 min in a vacuum. Compared to other SiC fibers, the TySA3 fibers exhibited remarkable thermal stability in the microstructure and no visible structural damage up to 1500 °C (Figs. 12(c)–(f)). Nevertheless, the TySA3 fiber exposed at 1800 °C had a rough surface and a porous structure near the fiber surface; nonetheless, the central parts of the fibers still had a relatively dense structure (Fig. 12(g)). Fig. 13 shows the EDS elemental mapping of TySA3 in the cross-section after exposure at 1800 °C for a holding time of 10 min in a vacuum. TySA3 was covered with a 1 μm-thick layer of carbon at the edge portions and SiC remained at the core.

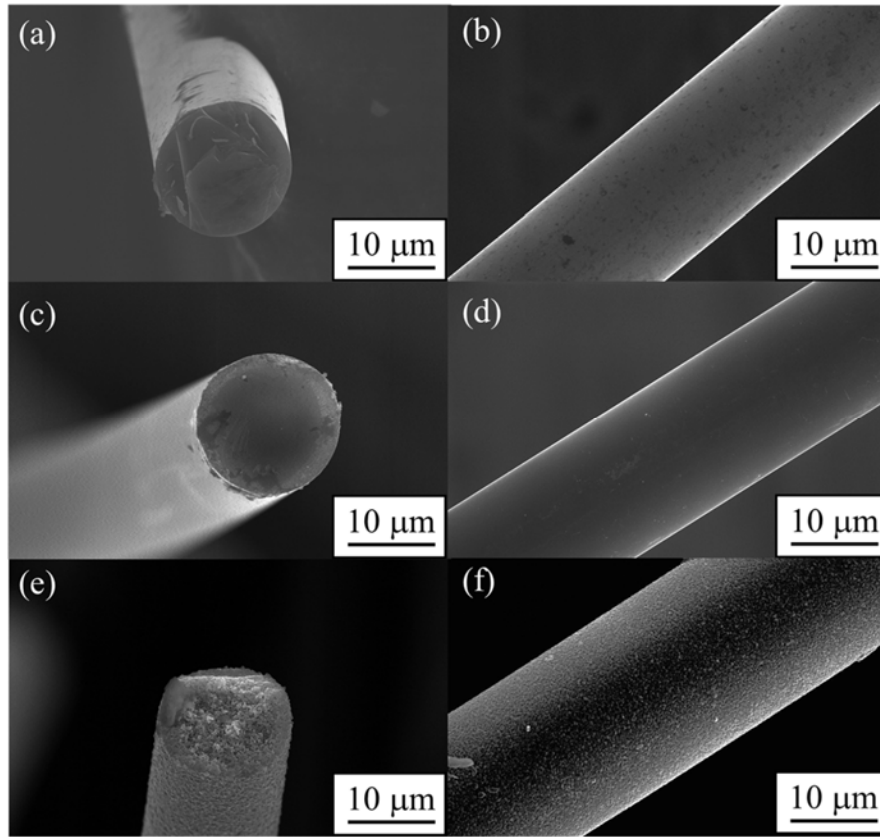


Fig. 9 Morphology of N: (a), (b) before exposure; (c), (d) after exposure to 1200 °C (e), (f) after exposure at 1500 °C. Holding time, 10 min in a vacuum.

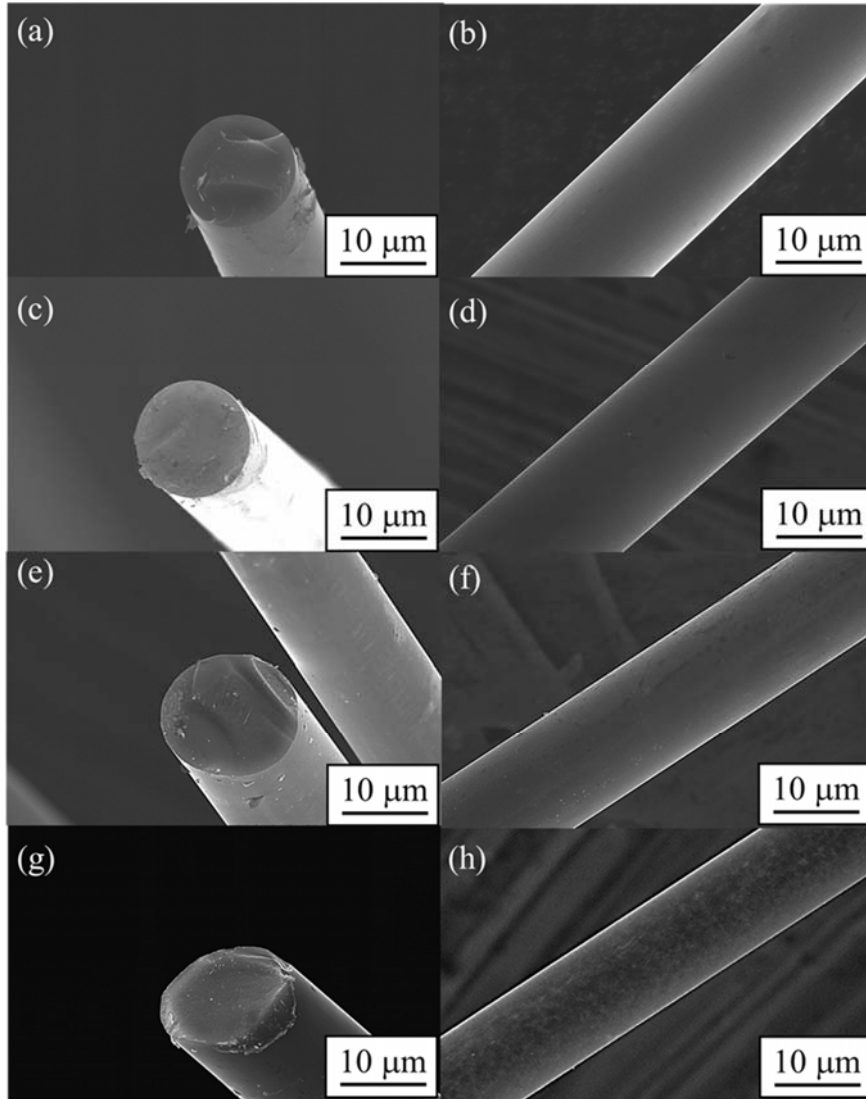


Fig. 10 Morphology of HN: (a), (b) before exposure; (c), (d) after exposure at 1200 °C; (e), (f) after exposure at 1500 °C; (g), (h) after exposure at 1800 °C. Holding time, 10 min in a vacuum.

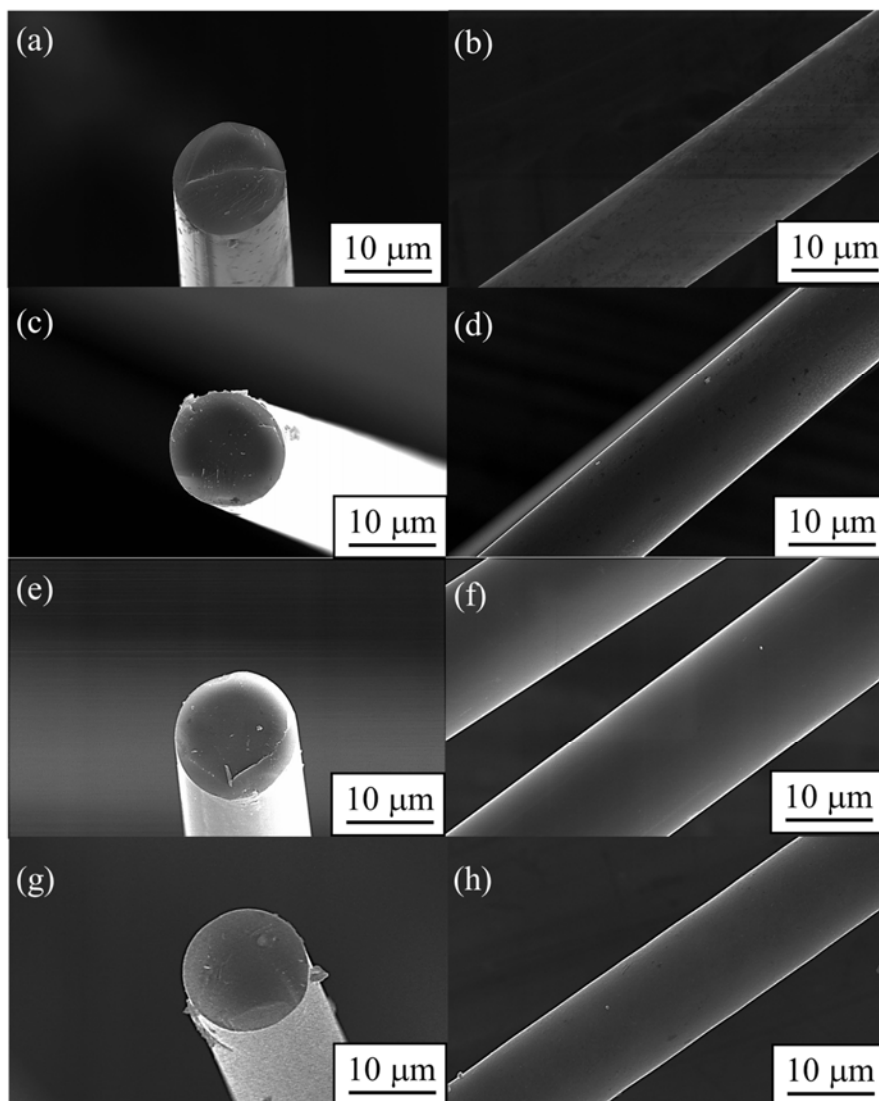


Fig. 11 Morphology of HNS: (a), (b) before exposure; (c), (d) after exposure at 1200 °C; (e), (f) after exposure at 1500 °C; (g), (h) after exposure at 1800 °C. Holding time, 10 min in a vacuum.

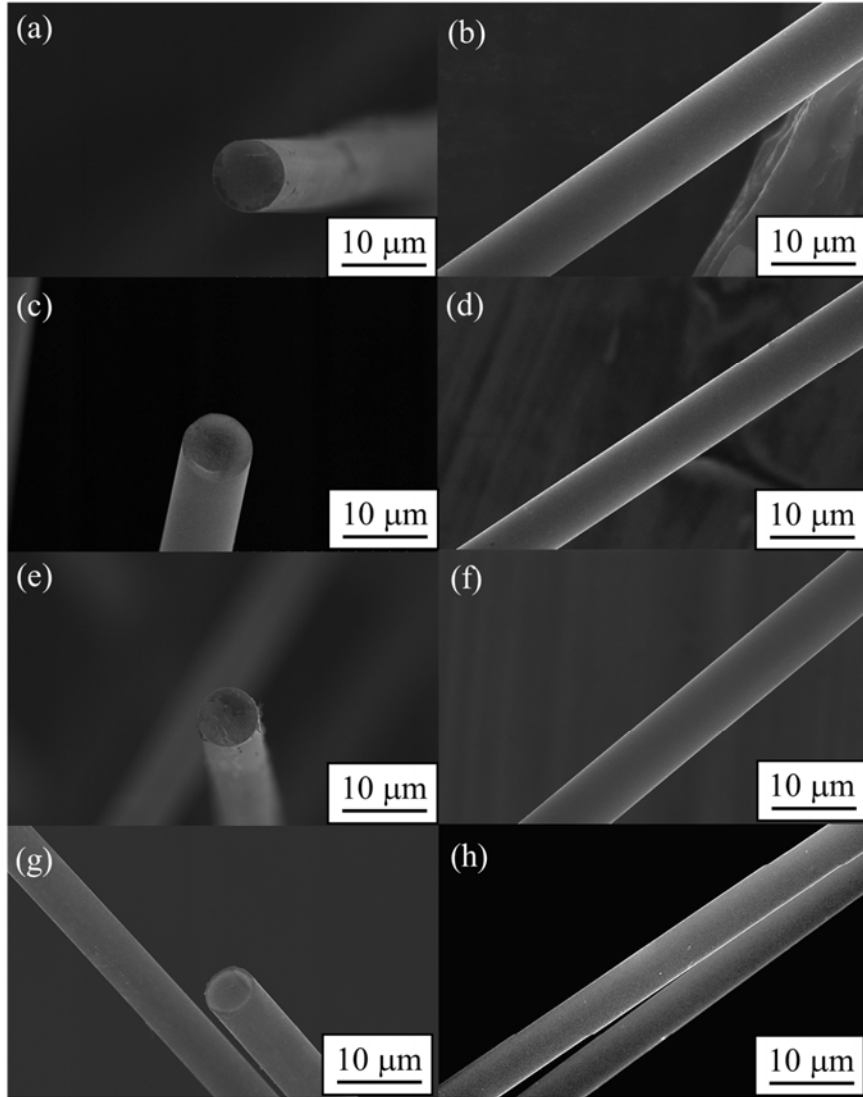


Fig. 12 Morphology of TySA3: (a), (b) before exposure; (c), (d) after exposure at 1200 °C; (e), (f) after exposure at 1500 °C; (g), (h) after exposure at 1800 °C. Holding time, 10 min in a vacuum.

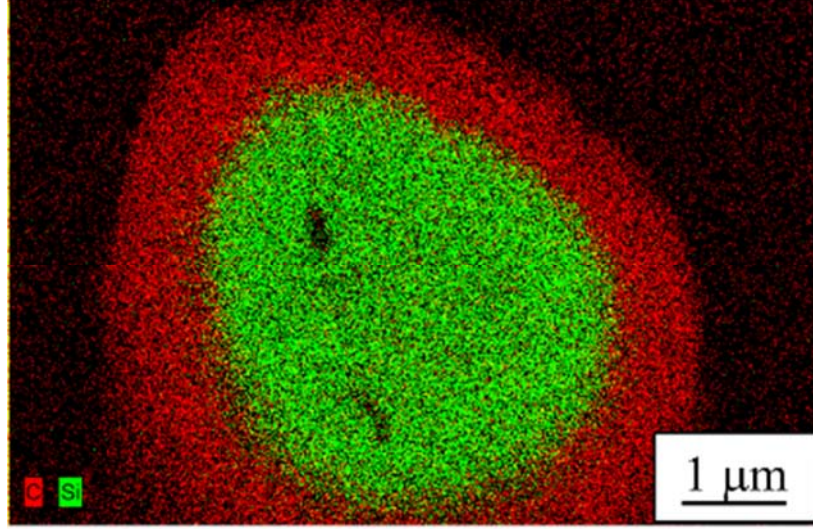


Fig. 13 EDS elemental mapping profile of TySA3 at the cross-section after exposure at 1800 °C for a holding time of 10 min in a vacuum.

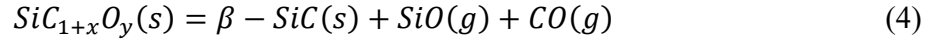
4. Discussion

Recently, Snead et al. proposed an empirical law to describe the elastic modulus (E) as a function of the temperature (Eq.3) [29].

$$E = E_0 - B T e^{-\frac{T_0}{T}}, \quad (3)$$

where B (GPa/K) and T_0 (K) are constants, T is the temperature (K), and E_0 is the elastic modulus at 0 K (assumed to be identical to that at room temperature). From the results of the experiments on bulk polycrystalline SiC, Snead et al. recommended 460 GPa for E_0 , 0.04 GPa/K for B , and 962 K for T_0 . Considering the uncertainties associated with Snead's model, predictions and experimental data are in good agreement between room temperature and 1500 °C. Snead's model followed by Eq. 3 was in good agreement with our experimental data obtained on third-generation fibers (HNS and TySA3). In general, the mechanical/physical and electrical properties, such as elastic modulus and electrical conductivity are determined by the microstructure, and are particularly related to the crystallinity and grain size within fibers [30]. The first-generation (Si-C-O) fibers such as N, produced from the melt-spinning of PCS, thermal oxidation curing, and thermal

pyrolysis, are classified as amorphous ($\text{SiC}_{1+x}\text{O}_y$), and contain a high oxygen content and excess carbon. When the fiber is heated to temperatures greater than 1200 °C, it crystalizes to β -SiC, which is accompanied by the release of CO and SiO gases, as indicated by the following equation.



The tensile strength of fibers is greatly reduced owing to the structural destruction (porous structure) caused by the release of these gases and the growth of β -SiC grains. This phenomenon has been reported in numerous studies [28, 30–32]. *In situ* measurements of the properties of fibers such as N at elevated temperatures was difficult owing to the severe degradation of tensile strength, which resulted in a sudden rupture of the fiber at around 1400 °C. The complete decomposition of the amorphous ($\text{SiC}_{1+x}\text{O}_y$) phase involves a heavy weight loss of approximately 26% for N [28]. After exposure to 1500 °C, the weight loss of N reached 25.6%, indicating that complete decomposition occurred. Consequently, a technique was devised to cross-link the PCS-based fibers through electron-beam irradiation without the use of oxygen. The fibers produced by this technique are classified as second-generation fibers such as HN, which have considerably enhanced heat resistance, elastic modulus, and electrical conductivity in the temperature range of 1200–1500 °C. The substantial increase in heat resistance may have been caused by the reduction in the quantity of the amorphous ($\text{SiC}_{1+x}\text{O}_y$) phase containing oxygen, as shown in Figs. 4(c) and (d) and 5(c) and (d). According to the XRD results shown in Figs. 7 and 8, considerable growth of the apparent β -SiC crystallites was observed in HN at the temperature range of 1200–1500 °C. The growth of the apparent β -SiC crystallites can be attributed to the coalescence of β -SiC nanocrystals from the decomposition of the amorphous ($\text{SiC}_{1+x}\text{O}_y$)

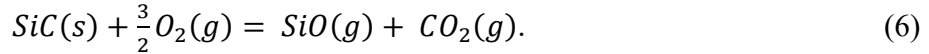
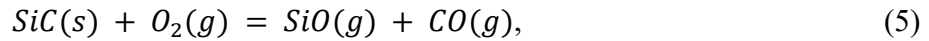
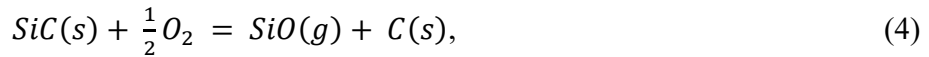
phase or the diffusion of Si and C atoms at the grain boundaries when exposed to high temperatures. The primary cause for the growth of apparent β -SiC crystallites would likely be the complete decomposition of the amorphous ($\text{SiC}_{1+x}\text{O}_y$) phase. The weight loss of HN reached 2.93% after exposure to 1500 °C, indicating that almost complete decomposition occurred (amorphous phase: approximately 3%) [28]. For bulk materials with pristine grain boundaries, grain growth occurs through the absorption of small grains by larger grains via grain boundary diffusion. In particular, grain boundary diffusion is much more efficient for small grains. Compared with TySA3, the growth of apparent β -SiC crystallites observed in HN and HNS is more obvious after exposure than before exposure (TEM images show that the grain size is approximately 5 nm for HN, 20 nm for HNS, 200 nm for TySA3) [33–35]. However, the residual trace oxygen may contribute to the Si and C grain boundary transport by accelerating diffusion since oxygen is not completely eliminated from the fiber, even in the HNS and TySA3 fibers, which are fabricated at very high temperatures [34, 36]. Taking into account the temperature for growth initiation of β -SiC crystallites (Fig. 8), the apparent β -SiC crystallite size might be primarily linked to the maximum temperature at which the fibers were fabricated. The fabrication temperatures of the HN, HNS, and TySA3 fibers are 1350, 1600, and approximately 1800 °C, respectively [37]. Furthermore, grain boundaries are defects that impede the movement of carriers, thus reducing their mobility. Consequently, larger grains lead to a lower density of defects and increased conductivity. This effect is especially noticeable when the grain size reaches the mean-free path of the carrier; a further increase in the grain size would lead to a significant increase in the conductivity. Evidently from Fig. 8, as expected, the apparent β -SiC crystallite size

increased when the exposure temperature was greater than the fabrication temperature, thereby resulting in an increase in the electrical conductivity. For HN, the degradation of mechanical/physical properties related to the growth of apparent β -SiC crystallites occurred at a relatively low temperature owing to the decomposition of the amorphous ($\text{SiC}_{1+x}\text{O}_y$) phase at approximately 1200-1500 °C, as shown in Figs. 2 and 3. As mentioned before, the initial β -SiC crystallite size in HN is considerably small; this is expected to induce high diffusivity at grain boundaries and result in significant growth of β -SiC crystallites upon exposure to high temperatures. Third-generation fibers with high crystallinity, a low oxygen content, and a nearly stoichiometric composition provided an extremely low quantity of the amorphous ($\text{SiC}_{1+x}\text{O}_y$) phase (approximately 1%) [28]. Hence, the thermal decomposition of the amorphous ($\text{SiC}_{1+x}\text{O}_y$) phase is largely negligible in HNS and TySA3. However, an unexpected phenomenon was observed between HN and HNS. Despite being the third-generation fiber, the apparent SiC crystallite size of HNS underwent larger growth than that of HN at 1800 °C, as shown in Fig. 8. This can be attributed to the excess carbon in HN. Takeda et al. investigated the properties of PCS-derived SiC fibers with various C/Si compositions and reported that the microstructure and mechanical properties depend considerably on the C/Si composition [38]. The increase in the amount of excess carbon in SiC contributed to the moderate growth of the apparent β -SiC crystallites for HN at 1800 °C. In other studies, growth inhibition due to excess carbon and the coalescence of the SiC microcrystals were also observed [39, 40]. Consequently, as shown in Fig. 5, the normalized electrical conductivity of HNS is almost the same as that observed during heating at the maximum temperature until 1500 °C owing to almost no grain growth. This

is in good agreement with the previous study [28]. Shimoo et al. reported that SiC crystallites in HNS with an extremely low quantity of the amorphous ($\text{SiC}_{1+x}\text{O}_y$) phase (1%) exhibited no growth at 1350–1450 °C for 1 h in a vacuum under a reduced pressure of 1 Pa because the growth of the β -SiC crystallites was primarily responsible for the decomposition of the amorphous ($\text{SiC}_{1+x}\text{O}_y$) phase [28]. In this study, the decomposition of the amorphous ($\text{SiC}_{1+x}\text{O}_y$) phase in third-generation fibers would not be completed at 1500 °C because the weight loss was 0.815% for HNS and 0.778% for TySA3. Hay reported that the amorphous ($\text{SiC}_{1+x}\text{O}_y$) phase in HNS was still observed using TEM after exposure to 1500 °C for 1 h in Ar–O₂ (P_{O_2} = 3.7 ppm) [27, 45]. TySA3 originally has very large SiC grains with an apparent crystallite size of 34.3 nm. In previous studies, TySA3 was reported to have a carbon-rich core, which results from the production process [36, 41, 42]. The grain size of SiC in the fiber core is considerably smaller than that in the edge region. This may be because carbon inhibited the growth of the apparent β -SiC crystallites. Additionally, this fiber contains a small amount of alumina (less than 1 wt%) as a sintering additive, which inhibits the significant growth of the apparent β -SiC crystallites as well. As a result, the TySA3 exhibited remarkable thermal stability in a vacuum below 1500 °C as well as HNS. We now consider the surface degradation of TySA3 when exposed to 1800 °C (Fig. 12(g) and (h)). As shown in Fig. 13, after exposure at 1800 °C, TySA3 consists of two distinct parts: the core and annular region. The microstructure of the core was unaffected; EDS elemental mapping revealed that the annular region was composed of pure carbon. In addition, the formation of carbon only after exposure to 1800 °C was confirmed through the XRD patterns, as shown in Fig. 7(d). The diameter of the fiber remained almost unchanged.

These findings indicate that Si volatilized. In this study, exposure was carried out in the chamber under a pressure lower than 10^{-4} Pa, which was lower than that of Si (g) at temperatures above 1400 °C [43]. This was in good agreement with results reported by Sauder et al., who investigated the creep properties of third-generation SiC fibers above 1400 °C [44]. For TySA3, this may be the reason for the gradual increase in electrical conductivities during heating and the marginal increase in electrical conductivities during cooling after exposure at 1500 and 1800 °C. In this study, based on the XRD and SEM results, the carbon layer was not detected in the annular region after exposure at 1500 °C; this is probably owing to the brief holding time of 10 min. Although the carbon layer was not observed for HNS owing to the larger fiber diameters or lower fiber roughness than those of TySA3, the release of Si from the fiber surface (i.e., Si sublimation) was likely caused by the exposure to 1800 °C. This is because the normalized electrical conductivity during cooling was higher than that during heating at 1800 °C, as shown in Fig. 5(f). It is quite important to strive to identify the optimal fabrication temperature that will yield both superior thermal stability and excellent mechanical strength. Hence, the upper limits of the fabrication temperatures are typically determined by the temperatures at which the fibers start to undergo performance degradation. Numerous studies have reported that fiber strength is affected by various factors: test temperature, holding time, total pressure, oxygen partial pressure, as well as dry and wet conditions [8, 9, 26–28, 45–47]. For instance, Takeda et al. found that HNS was chemically quite stable after exposure to Ar at 1600 °C for 10 h because structural decomposition did not occur, and HNS exhibited a high strength of approximately 1.9 GPa [8]. The strength retention of HN and HNS after 10 min exposure in a vacuum was marginally lower than that after 1 h exposure in Ar reported by

Sha et al.; however, the strength retention behavior of TySA3 was markedly different [26]. Shimoo et al. reported that the strength retention of SiC-based ceramic fibers after exposure at 1350–1450 °C decreased with the reduced total pressure [28]. HN and HNS after exposure to 1450 °C in a vacuum under a total pressure of 1 Pa had tensile strengths of 1.2 and 0 GPa, respectively [28]. The strength retentions of HN and HNS after 10 min in a vacuum were higher than those after 1 h in a vacuum. It is suspected that the active oxidation of SiC associated with holding time at a maximum test temperature causes severe degradation in strength. At high temperatures and low oxygen particle pressures, SiC is oxidized in an active oxidation regime via the following reactions:



Because the oxidation product SiO is a volatile material, the active oxidation of SiC causes significant weight loss and no oxide film is formed. Shimoo et al. reported that significant weight loss of 47.3% for HN and 62.7 % for HNS due to the decomposition of the amorphous ($\text{SiC}_{1+x}\text{O}_y$) phase followed by the active oxidation of SiC occurred after 1 h exposure to a vacuum at 1450 °C, resulting in severe strength degradation [28]. In this study, the weight loss for HN, HNS, and TySA3 at 1500 °C was insignificant, i.e., 2.93%, 0.815%, and 0.778%, respectively, owing to the extremely short holding time of 10 min in a vacuum. This indicated that the little active oxidation with insignificant weight loss occurred at 1500 °C, resulting in improved strength retention. Thus, microstructural evolutions and property changes based on the holding time at high temperatures should be

studied to further enhance lifetime. At 1800 °C, all the fibers showed significant weight loss of approximately 20%, which exceeded the complete decomposition of the amorphous ($\text{SiC}_{1+x}\text{O}_y$) phase, resulting in noticeable strength degradation, as shown in Fig. 6. Active oxidation may have occurred, but strength degradation was not significant. Thus, it was suspected that the strength degradation at 1800 °C was caused by the increased surface roughness during active oxidation and Si sublimation [27, 47], as shown in Figs. 10–12(h). The strength retention of TySA3 after 10 min exposure in a vacuum was considerably limited in relation to that after 1 h exposure in Ar. In addition, this limitation of tensile strength retention could be due to the formation of pure carbon in the annular region, with the volatilization of Si from the fiber surface as a major factor. The volatilization of Si from the fiber surface was limited to a high vacuum environment at 1800 °C, so it is not a critical issue for dense composites or composites with dense coatings, where the fiber reinforcements are not exposed in the advanced nuclear fission, fusion, nor aircraft applications below 1500 °C. Conversely, for FCI applications, expected at immediate temperatures of approximately 1000 °C, third-generation fibers such as HNS and TySA3 exhibited excellent strength stability and microstructures with small thermo-mechanical/physical and electrical property changes even at 1500 °C, as shown in Figs. 4 and 5(c) and (d). Although SiC is generally a fairly strong gap semiconductor, the electrical conductivity of various SiC-based ceramic fibers as a function of test temperature was considerably lower than that in pure SiC semiconductors, as shown in Figs. 3 and 5. The electrical conductivities of various SiC-based ceramic fibers negligibly depend on the electron transfer inside the SiC grains; however, it might suggest that it is affected by the amorphous phase within the fiber, grain boundaries, and/or free carbon networks. The

findings of this study are valuable for the future design and application of SiC-based composite materials and provide valuable insights into the strength stability and microstructure of SiC-based ceramic fibers at elevated temperatures.

5. Conclusions

The heat resistance of four commercial SiC-based ceramic fibers from three generations was evaluated using the single fiber tensile test device (MacaSiC) over a high-temperature range of 25–1800 °C in a vacuum under a pressure of less than 10^{-4} Pa. The *in situ* mechanical/physical and electrical properties, namely, elastic modulus and electrical conductivity, of the three generations of the SiC fibers were monitored during heating and cooling at 1200, 1500, and 1800 °C for 10 min. The findings were discussed in relation to fiber crystallinity and microstructural evolution. The key findings of this study are summarized as follows.

- (1) The first-generation fibers (N), which are amorphous and have a high oxygen content and excess carbon, became porous with crystallization to the amorphous ($\text{SiC}_{1+x}\text{O}_y$) phase when heated above 1200 °C. The elastic modulus rapidly decreased and the electrical conductivity increased above 1200 °C, and the fiber then suddenly ruptured at around 1400 °C.
- (2) The second-generation fibers (HN), which have low crystallinity, low oxygen content, and excess carbon, exhibited a considerable increase in heat resistance, elastic modulus, and electrical conductivity in the temperature range of 1200–1500 °C in relation to N. The considerable increase in heat resistance may have been due to the reduction in the quantity of the amorphous ($\text{SiC}_{1+x}\text{O}_y$) phase containing oxygen, but the mechanical properties

began to deteriorate owing to the low crystallinity at temperatures above 1200 °C. At temperatures at 1500 °C, the electrical conductivity increased rapidly owing to the accelerated growth of the apparent β -SiC crystallites involving the almost complete decomposition of the amorphous ($\text{SiC}_{1+x}\text{O}_y$) phase. Thus, the behavior of the elastic modulus and electrical conductivity during cooling was considerably different from that observed during heating at 1500 °C and 1800 °C.

(3) The third-generation fibers (HNS and TySA3), which have a high degree of crystallinity with low oxygen content and nearly stoichiometric composition, exhibited remarkable thermal stability to enable the measurement of the elastic modulus at up to 1800 °C; the elastic modulus was approximately 40% of its original value (that at room temperature, 25 °C). The electrical conductivity gradually increased up to 1800 °C. The normalized electrical conductivity value of HNS was higher than that of TySA3 during heating because of the gradual growth of the apparent β -SiC crystallites above 1500 °C. Despite TySA3 exhibiting almost no grain growth up to 1800 °C, the electrical conductivity of TySA3 during cooling was much higher than that during heating. This could be due to carbonization caused by the release of Si from the fiber surface after exposure at 1800 °C.

This study demonstrates the third-generation fibers such as HNS and TySA3 exhibited excellent strength stability and microstructures with small thermo-mechanical/physical and electrical property changes even at 1500 °C because the volatilization of Si from the fiber surface was limited to a high vacuum environment at 1800 °C. These findings contribute to the future design and application of SiC-based composite materials at elevated temperatures.

Acknowledgments

Mr. Giovanni Péan, and Ms. Hiromi Yoshihara and Masako Kato from NIMS supported us with FE-SEM observation and XRD analysis. The authors would also like to acknowledge Editage (www.editage.com) for their assistance with English language editing.

Funding

This work was partially supported by the Innovative Science and Technology Initiative for Security (Grant number JPJ004596), ATLA, Japan.

References

- [1] S. Yajima, Y. Hasegawa, K. Okamura, T. Matsuzawa, Development of high tensile strength silicon carbide fibre using an organosilicon polymer precursor, *Nature*. 273 (1978) 525–527. <https://doi.org/10.1038/273525a0>.
- [2] A.R. Bunsell, A. Piant, A review of the development of three generations of small diameter silicon carbide fibres, *J. Mater. Sci.* 41 (2006) 823–839. <https://doi.org/10.1007/s10853-006-6566-z>.
- [3] T. Ishikawa, Recent developments of the SiC fiber Nicalon and its composites, including properties of the SiC fiber Hi-Nicalon for ultra-high temperature, *Compos. Sci. Technol.* 51 (1994) 135–144. [https://doi.org/10.1016/0266-3538\(94\)90184-8](https://doi.org/10.1016/0266-3538(94)90184-8).
- [4] K. Kumagawa, H. Yamaoka, M. Shibuya, T. Yamamura, Thermal stability and chemical corrosion resistance of newly developed continuous Si-Zr-C-O tyranno fiber, *Ceram. Eng.*

- Sci. Proc. 18 (1997) 113–118 <https://doi.org/10.1002/9780470294437.ch12>.
- [5] K.M. Prewo, J.J. Brennan, G.K. Layden, Fiber-Reinforced Glasses and Glass-Ceramics for High-Performance Applications, *Am. Ceram. Soc. Bull.* 65 (1986) 305–314.
- [6] Y. Imai, Y. Tanaka, H. Ichikawa, T. Ishikawa, Development of advanced SiC/Al composite materials. Manufacturing of preform wires by liquid metal infiltration, *J. Iron. Steel. Inst. Jpn.* 75 (1989) 1555–1562.
https://doi.org/10.2355/tetsutohagane1955.75.9_1555.
- [7] K. Okamura, T. Seguchi, Application of radiation curing in the preparation of polycarbosilane-derived SiC fibers, *J. Inorg. Organomet. Polym.* 2 (1992) 171–179.
<https://doi.org/10.1007/BF00696544>.
- [8] M. Takeda, J. Sakamoto, A. Saeki, H. Ichikawa, Mechanical and Structural Analysis of Silicon Carbide Fiber Hi-Nicalon Type S, *Ceram. Eng. Sci. Proc.* (1996) 35–42.
<https://doi.org/10.1002/9780470314876.ch2>.
- [9] T. Ishikawa, Y. Kohtoku, K. Kumagawa, T. Yamamura, T. Nagasawa, High-strength alkali-resistant sintered SiC fibre stable to 2,200 °C, *Nature.* 391 (1998) 773–775.
<https://doi.org/10.1038/35820>.
- [10] P. Wang, F. Liu, H. Wang, H. Li, Y. Gou, A review of third generation SiC fibers and SiC/SiC composites, *J. Mater. Sci. Technol.* 35 (2019) 2743–2750.
<https://doi.org/10.1016/j.jmst.2019.07.020>.
- [11] R.T. Bhatt, F. Sola', L.J. Evans, R.B. Rogers, D.F. Johnson, Microstructural, strength, and creep characterization of Sylramic™, Sylramic™-iBN and super Sylramic™-iBN SiC fibers, *J. Eur. Ceram. Soc.* 41 (2021) 4697–4709.
<https://doi.org/10.1016/j.jeurceramsoc.2021.03.024>.

- [12] R.T. Bhatt, F. Sola-Lopez, M.C. Halbig, M.H. Jaskowiak, Thermal stability of CVI and MI SiC/SiC composites with Hi-Nicalon™-S fibers, *J. Eur. Ceram. Soc.* 42 (2022) 3383–3394. <https://doi.org/10.1016/j.jeurceramsoc.2022.03.009>.
- [13] K. Shimoda, H. Kakisawa, Novel production route for SiC/SiC ceramic-matrix composites using sandwich prepreg sheets, *J. Eur. Ceram. Soc.* 43 (2023) 805–813. <https://doi.org/10.1016/j.jeurceramsoc.2022.11.005>.
- [14] K. Shimoda, T. Hinoki, Effect of BN nanoparticle content in SiC matrix on microstructure and mechanical properties of SiC/SiC composites, *Int. J. Appl. Ceram. Technol.* 20 (2023) 2466–2477. <https://doi.org/10.1111/ijac.14365>.
- [15] A. Patel, E. Sato, T. Takagi, N. Shichijo, Effect of oxidation on the bending fatigue behavior of an advanced SiC/SiC CMC component at 1000 °C in air, *J. Eur. Ceram. Soc.* 42 (2022) 4121–4132. <https://doi.org/10.1016/j.jeurceramsoc.2022.03.061>.
- [16] Y. Katoh, Ceramic matrix composites in fission and fusion energy applications, in: I.M. Low (Ed.), *Advances in Ceramic Matrix Composites*, second ed., Woodhead Publishing, 2018, pp. 595–622. <https://doi.org/10.1016/B978-0-08-102166-8.00024-4>.
- [17] H. Yu, X. Zhou, H. Wang, S. Zhao, Y. Wu, Q. Huang, Z. Zhu, Z. Huang, 2D SiC/SiC composite for flow channel insert (FCI) application, *Fusion Eng. Des.* 85 (2010) 1693–1696. <https://doi.org/10.1016/j.fusengdes.2010.05.004>.
- [18] S. Konishi, M. Enoda, M. Nakamichi, T. Hoshino, A. Ying, S. Sharafat, S. Smolentsev, Functional materials for breeding blankets—status and developments, *Nucl. Fusion.* 57 (2017) 092014. <https://doi.org/10.1088/1741-4326/aa7e4e>.
- [19] K.A. Terrani, Accident tolerant fuel cladding development: Promise, status, and challenges, *J. Nucl. Mater.* 501 (2018) 13–30.

<https://doi.org/10.1016/j.jnucmat.2017.12.043>.

[20] G. Singh, J. Gorton, D. Schappel, N.R. Brown, Y. Katoh, B.D. Wirth, K.A. Terrani, Deformation analysis of SiC-SiC channel box for BWR applications, *J. Nucl. Mater.* 513 (2019) 71–85. <https://doi.org/10.1016/j.jnucmat.2018.10.045>.

[21] F.W. Zok, Ceramic-matrix composites enable revolutionary gains in turbine engine efficiency. *J. Am. Ceram. Soc.* 95 (2016) 22–28.

[22] N.P. Padture, Advanced structural ceramics in aerospace propulsion, *Nat. Mater.* 15 (2016) 804–809. <https://doi.org/10.1038/nmat4687>.

[23] T. Nakamura, T. Oka, K. Imanari, K.-I. Shinohara, M. Ishizaki, Development of CMC turbine parts for aero engines, *IHI Eng. Rev.* 47 (2014) 29–32.

[24] J. Steibel, Ceramic matrix composites taking flight at GE Aviation. *Am. Ceram. Soc. Bull.* 98 (2019) 30–33.

[25] JIS R7606, "Determination of the tensile properties of the single filament specimens," Japanese Industrial Standards Committee. 2000.

[26] J.J. Sha, T. Nozawa, J.S. Park, Y. Katoh, A. Kohyama, Effect of heat treatment on the tensile strength and creep resistance of advanced SiC fibers, *J. Nucl. Mater.* 329–333 (2004) 592–596. <https://doi.org/10.1016/j.jnucmat.2004.04.123>.

[27] R.S. Hay, SiC fiber strength after low pO₂ oxidation, *J. Am. Ceram. Soc.* 101 (2017) 831–844. <https://doi.org/10.1111/jace.15198>.

[28] T. Shimoo, K. Okamura, H. Takeuchi, Effect of reduced pressure on oxidation and thermal stability of polycarbosilane-derived SiC fibers, *J. Mater. Sci.* 38 (2003) 4973–4979. <https://doi.org/10.1023/B:JMSC.0000004421.67094.2e>.

[29] L.L. Snead, T. Nozawa, Y. Katoh, T.-S. Byun, S. Kondo, D.A. Petti, Handbook of sic

- properties for fuel performance modeling, *J. Nucl. Mater.* 371 (2007) 329–377. <https://doi.org/10.1016/j.jnucmat.2007.05.016>.
- [30] K. Okamura, T. Shimoo, K. Suzuya, K. Suzuki, SiC-based ceramic fibers prepared via organic-to-inorganic conversion process-a review. *J. Ceram. Soc. Jpn.* 114 (2006) 445–454. <https://doi.org/10.2109/jcersj.114.445>.
- [31] T. Mah, N.L. Hecht, D.E. McCullum, J.R. Hoenigman, H.M. Kim, A.P. Katz, H.A. Lipsitt, Thermal stability of SiC fibres (Nicalon®), *J. Mater. Sci.* 19 (1984) 1191–1201. <https://doi.org/10.1007/BF01120029>.
- [32] D.J. Pysher, K.C. Goretta, R.S. Hodder Jr, R.E. Tressler, Strengths of Ceramic Fibers at Elevated Temperatures, *J. Am. Ceram. Soc.* 72 (1989) 284–288. <https://doi.org/10.1111/j.1151-2916.1989.tb06115.x>.
- [33] G. Chollon, R. Pailler, R. Naslain, F. Laanani, M. Monthieux, P. Olry, Thermal stability of a PCS-derived SiC fibre with a low oxygen content (Hi-Nicalon), *J. Mater. Sci.* 32 (1997) 327–347. <https://doi.org/10.1023/A:1018541030308>.
- [34] H. Ichikawa, Recent advances in Nicalon ceramic fibres including Hi-Nicalon type S, *Ann. Chim. Sci. Mat.* 25 (2000) 523–528. [https://doi.org/10.1016/S0151-9107\(01\)80004-0](https://doi.org/10.1016/S0151-9107(01)80004-0).
- [35] A.R. Bunsell, M.-H. Berger, Fine diameter ceramic fibres, *J. Eur. Ceram. Soc.* 20 (2000) 2249–2260. [https://doi.org/10.1016/S0955-2219\(00\)00090-X](https://doi.org/10.1016/S0955-2219(00)00090-X).
- [36] S.M. Dong, G. Chollon, C. Labrugère, M. Lahaye, A. Guette, J.L. Bruneel, M. Couzi, R. Naslain, D.L. Jiang, Characterization of nearly stoichiometric SiC ceramic fibres, *J. Mater. Sci.* 36 (2001) 2371–2381. <https://doi.org/10.1023/A:1017988827616>.
- [37] In *Comprehensive Composite Materials*. A. Kelly and C. Zweben; T.W. Chou, Eds.; Elsevier: Amsterdam, 2000; Vol. 1, p 107

- [38] M. Takeda, A. Saeki, J.-I. Sakamoto, Y. Imai, H. Ichikawa, Properties of polycarbosilane-derived silicon carbide fibers with various C/Si compositions, *Compos. Sci. Technol.* 59 (1999) 787–792. [https://doi.org/10.1016/S0266-3538\(99\)00009-3](https://doi.org/10.1016/S0266-3538(99)00009-3).
- [39] S. Yajima, K. Okamura, T. Matsuzawa, Y. Hasegawa, T. Shishido, Anomalous characteristics of the microcrystalline state of SiC fibres, *Nature*. 279 (1979) 706–707. <https://doi.org/10.1038/279706a0>.
- [40] Y. Sasaki, Y. Nishina, M. Sato, K. Okamura, Raman study of SiC fibres made from polycarbosilane, *J. Mater. Sci.* 22 (1987) 443–448. <https://doi.org/10.1007/BF01160751>.
- [41] M. Havel, Ph. Colomban, Skin/bulk nanostructure and corrosion of SiC-based fibres: a surface Rayleigh and Raman study, *J. Raman Spectrosc.* 34 (2003) 786–794. <https://doi.org/10.1002/jrs.1053>.
- [42] M. Havel, Ph. Colomban, Rayleigh and Raman images of the bulk/surface nanostructure of SiC based fibres, *Compos. Part B Eng.* 35 (2004) 139–147. [https://doi.org/10.1016/S1359-8368\(03\)00086-6](https://doi.org/10.1016/S1359-8368(03)00086-6).
- [43] P. Rocabois, C. Chatillon, C. Nernard, Thermodynamics of the Si-O-N System: I, High-Temperature Study of the Vaporization Behavior of Silicon Nitride by Mass Spectrometry, *J. Am. Ceram. Soc.* 79 (1996) 1351–1360. <https://doi.org/10.1111/j.1151-2916.1996.tb08596.x>.
- [44] C. Sauder, J. Lamon, Tensile creep behavior of SiC-based fibers with a low oxygen content, *J. Am. Ceram. Soc.* 90 (2007) 1146–1156. <https://doi.org/10.1111/j.1551-2916.2007.01535.x>.
- [45] R.S. Hay, R. Corns, A. Ross, B. Larson, P. Kazmierski, Fiber strength of Hi-NicalonTM-s after oxidation and scale crystallization in Si(OH)₄ saturated steam, *Ceram.*

Eng. Sci. Proc. 37 (2017) 109–119. <https://doi.org/10.1002/9781119320104.ch10>.

[46] R.S. Hay, R.J. Chater, Evaluation of SiC/SiC minicomposites with yttrium disilicate fibercoating, J. Am. Ceram. Soc. 100 (2017) 4110–4130. <https://doi.org/10.1111/jace.14833>.

[47] Y. Zhang, T. Chen, J. Chen, Q. Zhang, Y. Gou, The effects of annealing atmosphere and intrinsic component on high temperature evolution behaviors of SiC fibers, Mater. Sci. Eng. A. 848, 673 (2016) 143363. <https://doi.org/10.1016/j.msea.2022.143363>.

Table Captions

Table 1 Characteristics of various SiC-based ceramic fibers (data provided by manufacturers).

Table. 1 Characteristics of various SiC-based ceramic fibers (data provided by manufacturers).

| | Nicalon with low electrical resistivity (N) | Hi-Nicalon (HN) | Hi-Nicalon Type S (HNS) | Tyranno-SA 3 rd (TySA3) |
|-----------------------------|---|------------------------------------|-------------------------------|---|
| Diameter (μm) | 14 | 14 | 12 | 7.5 |
| Density (g/cm^3) | 2.4 | 2.65 | 2.85 | 3.1 |
| Atomic composition | $\text{SiC}_{1.34}\text{O}_{0.36}$ | $\text{SiC}_{1.39}\text{O}_{0.01}$ | $\text{SiC}_{1.05}$ | $\text{SiC}_{1.08}$, O, Al _{<0.01} |
| Crystal state | Amorphous | Micro crystal | Crystalline | Crystalline |
| Tensile strength (GPa) | 3.1 | 3.2 | 3.1 | 2.51 |
| Tensile modulus (GPa) | 190 | 270 | 380 | 409 |